Proceedings of Manufacturing Science and Engineering Conference 2021
MSEC 2021
June 21-25, 2021, Cincinnati, Ohio, USA

MSEC2021-63615

A STUDY OF THE EFFICACY OF FLAME ELECTRICAL RESISTANCE FOR STANDOFF MEASUREMENTS DURING THE OXYFUEL CUTTING PROCESS

Christopher R. Martin*

Altoona College
Penn State Unviersity
Altoona, PA

Alexandrina Untaroiu
Kemu Xu
S M Mahbobur Rahman
Department of Mechanical Engineering
Virginia Tech
Blacksburg, VA

ABSTRACT

This is a study of the suitability of preheat flame electrical resistance as a potential method for measuring the standoff distance an oxyfuel cutting torch and a work piece. Careful scrutiny of forty seven (47) individual experiments demonstrate that when cut quality is good, there is a linear repeatable relationship between the two with uncertainty about $\pm$ .3mm (.015in). As the cut quality degrades, the formation of top-edge dross reduces the electrical path length in the flame, and momentary reduction in the reaction rate in the kerf reduces the free electrons in the flame, causing rises in flame resistance. In these conditions, measurement uncertainty reduces to $\pm$ 1mm (.040in) or worse.

1 Introduction

This study identifies non-ideal aspects of the preheat flame electrical resistance while performing oxyfuel cuts of steel plates. Previously proposed as a method for measuring the standoff distance (distance between torch and work), this signal has been more recently shown to exhibit sensitivities to other process parameters as well [1, 2]. The present study establishes the physical mechanisms for changes in measured flame resistance not due to changes in standoff. The results of this study are the next logical step to addressing the question of whether flame resistance is a viable flame electrical characteristic for inferring standoff.

Despite over a century as a widespread standard method for cutting steel plate, oxyfuel cutting remains notoriously difficult to fully automate. Though large multi-torch mechanized oxyfuel systems have been in standard use for decades, persistent shortcomings in their sensing suites still mandate the attention of a skilled operator to ensure preheat times, torch heights, and gas mixtures are appropriate. Sensing suites exist for these systems, but there are countless anecdotes of operators removing them in favor of manual operation due to their unreliability. The core of the problem is twofold:

1. The process is loud, radiative, abrasive, noisy, and is consequently abusive to sensors.
2. The cut quality (and even cut failure) is heavily dependent on the temperature of the work piece, so consistent quality cuts must either adapt to the local state of the work piece in real time, or the operator must take appropriate measures to ensure that the process parameters are adjusted appropriately.
3. The presence of combustion gases, metal dust, and other process byproducts can interfere with the fundamental physics underlying many sensing systems, causing measurement uncertainty.

The result is that the oxyfuel cutting process is often uninstrumented. For example, when the torch height is measured at all, the industry has converged to capacitive sensors to detect the standoff distance between the work and the torch, but there is a distinct absence of independent assessment of these systems

*Email: crm28@psu.edu

Copyright © 2021 by ASME

in the literature. Most manufacturers do not document their sensor uncertainty, but Messer's *Sensomat-PAN* capacitive system claims ±3mm (0.12in) uncertainty with ±1mm (0.04in) repeatability [3].

This challenge is magnified by the widespread use of parallel torches operating simultaneously on the same work piece to increase throughput. Torches operating on parallel parts must all pierce at the same time and cut at the same speeds; whether or not the work under them is at the same conditions. Gantries carrying 12 or even 24 torches simultaneously are not uncommon.

1.1 Ion Current Sensing

The idea of sensing by passing electrical currents through the oxyfuel cutting preheat flame is over sixty years old [4], but has never been successfully commercialized. The approach is attractive, since it promises to provide vital information about the cutting process without the addition of vulnerable sensors. Still, persistent questions regarding the underlying physics that influence these signals have been obstacles to their use until recently.

The study of the formation and transport of the ions that form naturally in flames has been a mater of widespread study in combustion and thermal fluid science, and the authors have already published a number of surveys of the characteristics that are peculiar to the oxyfuel flame. A surveys of the low frequency current-voltage characteristics are available while preheating [1,5,6,7], and while cutting [2,8]. Measurements of the electrical structure of the flame confirmed that the formation and rapid recombination of ions in the flame's inner cone are responsible for *primary* electrical currents [9], and *secondary* electrical currents are caused by chemical action at the work surface [5]. Detailed computational [10] and analytical [11] models confirm the importance of charged *sheaths* at the metal surfaces for the semiconductor characteristics of the flame.

Figure 1 shows example current-voltage characteristics of the oxyfuel flame measured while cutting published in [2]. In all of these studies, the table and work are grounded and signals are applied to the torch and through the flame. Each data set is shown at a different times during the test: 30 seconds was during preheat, 35 seconds was immediately after pierce, 65 seconds is at a near-loss-of-cut event, 90 seconds is after the cut was able to recover, and 110 seconds is after the flame has left the plate. While it stands to reason that it should be more difficult to pass electrical currents through a wide gap than through a short one, Figure 1 demonstrates how heavily nonlinear the system can be.

At both high- and low-voltages, the flame *saturates*, causing the current-voltage characteristic to deviate from the ideal linear behavior if a resistor. There is also a *floating potential* which is known to drift throughout the preheat and cutting process. Realistic cutting conditions require a rich flame, but nearer to stoichiometric conditions, the left-hand (negative voltage) saturation currents grow to be many times the levels seen here, just as the

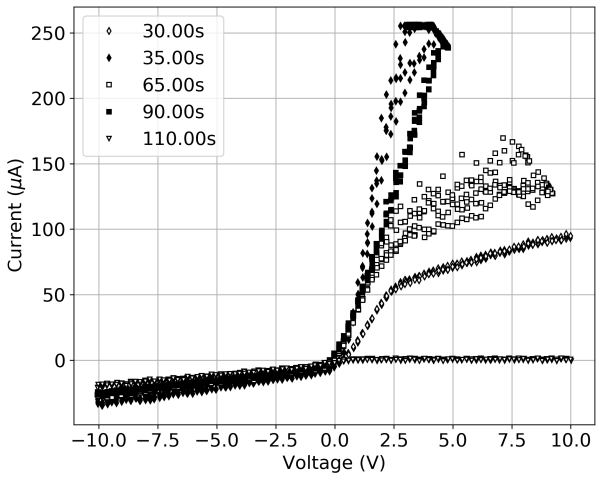

FIGURE 1. Example current-voltage characteristics of an oxyfuel preheat flame taken from [2]

right-hand (positive voltage) saturation can be seen to vary while cutting. All of these nonlinearities have been demonstrated to be due to sheaths that form in the vicinity of the torch tip and work surface [11].

In the small region between positive and negative saturation, the IV characteristic adopts a linear behavior, which we have previously called *Ohmic*. There is mounting evidence that even this regime of the IV characteristic is not entirely linear [11], but for the sake of this study, it is practical to call that slope the flame's net electrical resistance, even if it still includes aspects of the sheaths' nonlinear IV characteristics.

From this body of work the flame's ohmic resistance appears to be the most promising method for measuring standoff, but no thorough investigation of its suitability for the task exists in the literature. Though the predominant physical mechanisms for the flame's electrical characteristics have been identified, and models exist to provide reasonable predictions for the flame's characteristics, it has not yet been established whether the cutting process yields complicating factors that may corrupt the measurement's integrity.

In this experimental study of the flame resistance method for measuring torch standoff, two mechanisms are identified that degrade the measurement's uncertainty as cut quality is degraded, and the measurement uncertainty is quantified in good and poor cutting conditions.

2 Experiment

To test the variation of flame resistance with standoff, a series of 47 data sets were collected over mild steel plates that were deliberately set at a slope relative to the torch motion. Plates were placed on three adjustable points of contact that could be

Copyright © 2021 by ASME

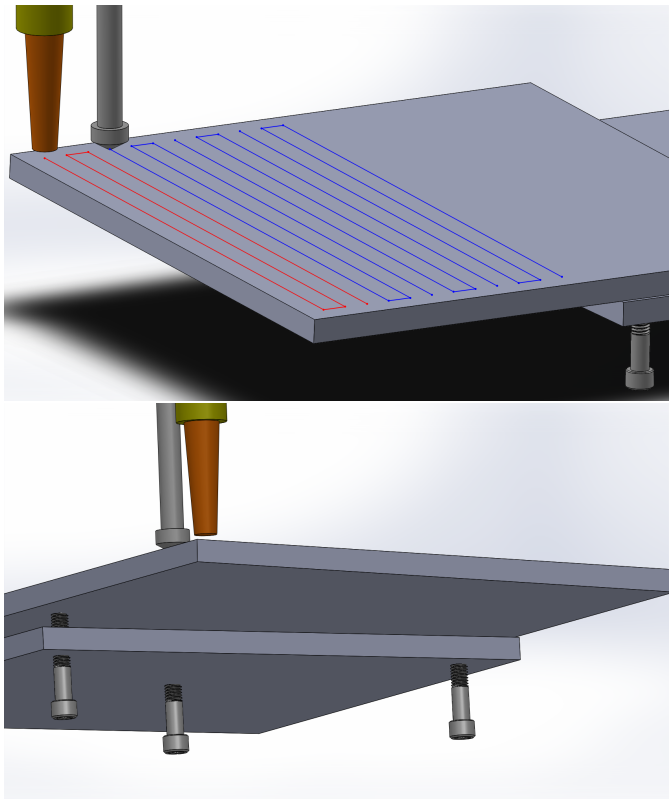

FIGURE 2. CAD models for the experiment with three-pass paths outlined in red and blue. In the bottom view, the three-point-of-contact screw adjustment is shown.

adjusted to control the plate's pitch and roll, shown in Figure 2. Weight was added as needed (not shown) to bias the work piece against the three adjustment points. Each data set is comprised of a series of cuts along the plates' roll direction. Prior to every test, the clearance between the torch and the plate was measured at the high and low side, and the roll was adjusted until the low-standoff (high-side) was at or below about 2.5mm (0.1in) and the high-standoff (low-side) was about 6.4mm (.25in).

Torch motion was controlled by a Silhouette 500 cutting machine modified for CNC. Work pieces were 300mm (12in) square and 12.7mm (1/2-inch) thick or 6.4mm (1/4-inch) thick. Cuts were performed with a pierce operation near one end of the plate, followed by a 2-second dwell for the pierce to complete, finished by a series of one, two, or three 279mm (11in) passes up and down the slope of the plate. As shown in Figure 3, each pass was offset by the one previous by 12.7mm (0.5in), forming an elongated "C" (for two passes) or "S" (for three passes). Cuts were started at high- and low-standoff, but tests started at low standoff were more likely to damage the torch tip. In the vast majority of data sets with multiple passes, the torch was advanced along the plate by 12.7mm (.5in).

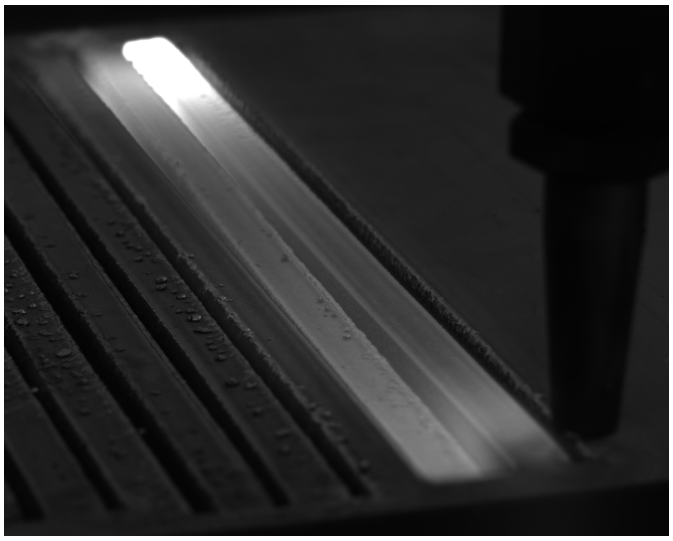

FIGURE 3. An image in visible + NIR of a plate immediately after a test. These tests are relatively poor quality cuts with significant top-edge dross.

All data, meta-data, and post-processing from each test were collected into a directory named with a 14-digit time stamp (YYYYmmDDHHMMSS) representing the time at which the test began. The last four digits (minuts + seconds) were used to uniquely identify each test. In the rare instance that two tests have the same last four digits, a fifth is used.

2.1 Standoff Measurement

In previous tests, errors due to curvature of the plate and motion of the plate during the cut were on the same order of magnitude as the test-to-test variation [2]. To compensate for these phenomena, a water-cooled standoff probe was dragged along the top of the plate 38.1mm (1.5in) from the centerline of the torch axis. Shown in Figure 2, the probe was constructed of concentric 1/2-inch and 1/4-inch stainless steel tubes with a conical stainless steel tip brazed to the outer tube. The entire actively cooled assembly was allowed to float vertically in self-lubricating linear bearings (not shown) on a ceramic-coated aluminum shaft concentric with the cooled tubes. Aluminum plates 6.4mm (.25in) thick were milled to form clamps with epoxied alumina balls forming six electrically insulating points of contact on the torch body. The vertical motion of the probe relative to the torch was monitored by a precision linear potentiometer.

The probe was calibrated by manually moving the torch above a target clamped to the table below. A dial indicator was similarly clamped so that its probe lay on the manifold alongside the linear potentiometer. In these measurements, some effort was made to deliberately bias the probe side-to-side to induce the same forces on the tip as may be produced during a

Copyright © 2021 by ASME

cut. The measurements were found to be linear and repeatable to within .05mm (.002 inches), consistent with the potentiometer manufacturer specifications.

Prior to each cut, a gauge plate either 2.54mm (.1in) or 6.35mm (0.25in) was placed on the plate and the torch height was adjusted to touch. All subsequent standoff sensor voltages were adjusted so that this initial value matched the known offset. Pessimistic estimates of the initial offset precision are roughly +/- .5mm (.02in) based on variations in the torch angle relative to the plate, bend in the arm supporting the torch, and variations in roughness of the torch tip and plate surface. Experimental technique improved to tighten controls in later experiments.

The plate was found to move on the order of .5mm or .02in or more during preheat and pierce operations. Furthermore, even if plates were flat prior to cutting, plate warp was clearly evident in some tests.

2.2 Flame Resistance Measurement

The flame's electrical resistance was measured by monitoring voltage while imposing a 5-15μA 10Hz sine wave with positive current leaving the torch (electrons leaving the work). Resistance is calculated by calculating the ratio of the amplitudes of the fast-fourier-transforms (FFT) of voltage and current at the 10Hz excitation frequency.

This technique for measuring the electrical resistance of the flame was first presented in [2], and was shown to effectively mitigate error due to noise and floating potential drift. While there is some evidence that the measurement may not entirely eliminate the nonlinear semiconductor aspects of the flame [11], it has been demonstrated quite clearly that the dominant component of the signal is the flame's electrical resistance [1, 5, 2].

To monitor for corruption of the data due to the rise of nonlinearities, [2] also established the practice of monitoring the first two super-harmonics of the fundamental frequency (20 and 30Hz in this case). In this study, measurements were taken of the voltage, current, and standoff at 2kS/s, and the FFTs were performed over one-second (2000-sample) windows. This provided a frequency resolution of 1Hz, and data above 500Hz were ignored as improperly sampled.

Voltage and current were measured by a LabJack T7 ethernet DAQ interfacing with a custom amplifier circuit. Analog signals proportional to voltage and current were calibrated against a Keysight precision multimeter. Current measurements over a $\pm$100μA range were calibrated within $\pm$.1μA. The most extreme deviation occurred at the measurement's maxima, with errors less than .05μA typical over the rest of the range. Common mode rejection tests of the current measurement were conducted over the circuit's entire $\pm$10V range with 77.5dB rejection, meaning that changes in torch voltage did not erroneously couple into the torch current signal. The 1:1 voltage buffer was found to replicate the torch voltage from -10 to +10V to within 7mV with errors less than 2mV typical over most of the range. The current command was generated using the DAQ's onboard DAC output to far less precision, but the actual measured output values were recorded instead of trusting the amplifier's calibration.

2.3 Experimental Conditions

An Oxweld C-67 machine cutting torch was used with 1/2-inch low-speed two-part tips. To measure the impact of preheat flow rates, cuts were performed with high (16.8L/min or 35scfh) and low (12.9L/min or 27scfh) preheat gas flow rates. Most tests included here were performed with a preheat fuel/oxygen ratio 0.77, but some tests were performed with 0.80 to investigate the importance of mixture. Tests were also performed with nominal (3.1bar or 45psig) and high (5.2 or 75psig) cutting oxygen pressure.

The flow rates were adjusted by metering valves and monitored by thermal mass flow meters in gas supplies lines in a separate room from the experiment. This eliminated any risk of flow rate drift due to thermal effects.

2.4 Infrared Photography

Over the course of these measurements, it became apparent that monitoring the state of top-edge dross would be necessary. For this purpose, a ThorLabs DCC3240N (a rebranded IDS UI-3240CP-NIR) camera was used to collect video throughout the cut. The camera sensitivity includes the visible spectrum through about 1000μm, which was more than sufficient to allow the kerf to self-illuminate. With a one-inch machine vision lens, a pinhole aperture, and an exposure time around 50μs, images of the molten dross were well formed.

3 Results

The 47 data sets represent a wide range of operating conditions with far too much nuance in their data to present in a single plot. Instead, the results are grouped by phenomenology to attempt to communicate the patterns that emerged as clearly as possible. All tests were carefully analyzed for consistency with the arguments we present here, but some were excluded due to errors in the test (e.g. incursion with slag formed by previous cuts, standoff probe hanging on features in the plate surface, or loss of cut).

3.1 Results from successful cuts

Cuts on 12mm (1/2-inch) steel plates at low preheat flame (12.9L/min), nominal cutting oxygen pressure (3.1bar), and a feed rate of 406mm/min (16ipm) produced excellent cuts with low dross. Figure 4 shows the flame resistance plotted against standoff for three data sets, each of which contains three passes,

Copyright © 2021 by ASME

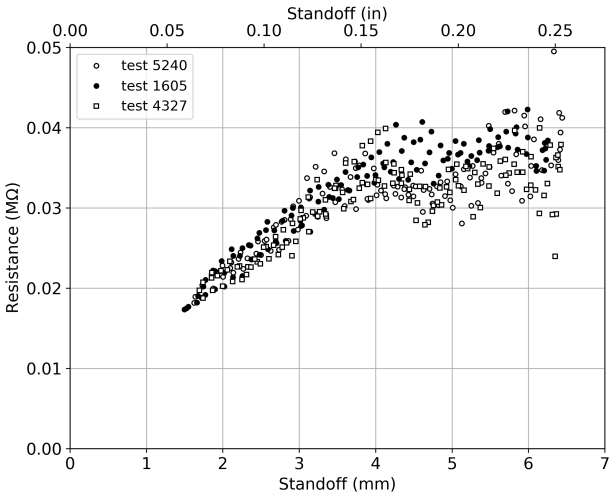

FIGURE 4. Resistance versus standoff; 1/2-inch steel, 406mm/min, low preheat, nominal cutting oxygen

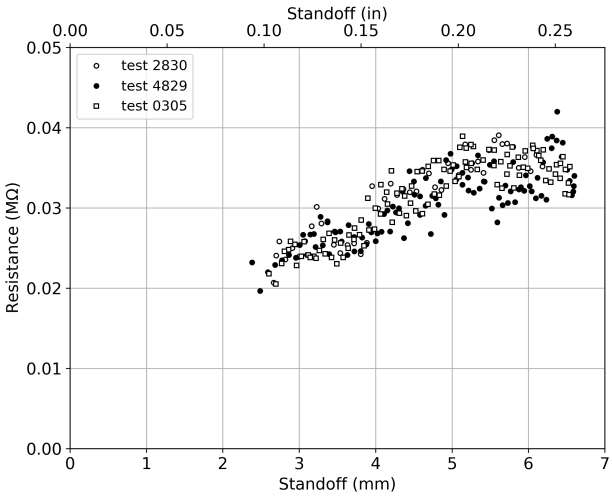

FIGURE 5. Resistance versus standoff; 1/2-inch steel, 305mm/min, low preheat, high cutting oxygen

so there are nine passes represented with no control on the plate temperature. These data demonstrate excellent linearity and repeatability, but only at low standoffs. Ideal standoff for these conditions is around 3mm (.125in).

The following data represent deliberate deviations from these conditions to asses their impact on the measurement. Identical cuts with high cutting oxygen pressure (5.2bar) and a lower feed rate (305mm/min or 12ipm) produced light top-edge dross and heavy low-speed dross on the underside of the cut. Figure 5 shows three tests conducted under these conditions; one with a single pass and the other two with two passes, so that five passes are represented in these data. These conditions produce similar repeatable data without the flat region at high standoff, with a slightly lower resistance, and a less clearly defined slope.

Figure 6 shows two data sets with high cutting oxygen pressure (5.2bar) and high preheat flow rate (16.8L/min). These conditions produced poor cuts with substantial top-edge rounding, top-edge dross, and large globs of tenacious bottom-edge dross. These data adopt a repeatable linear behavior but with substantially more scatter. The groupings of data points tempt the conclusion that there is a hysteresis loop, but that is not the case; the upper and lower edges of the data are alternating.

Figure 7 shows data collected while cutting with nominal cutting pressure, at high preheat, but two of the five data sets have fuel/oxygen mixtures (0637 and 1950) increased to 0.80 from the nominal 0.77 used in all other tests. Test 1043 was conducted with a 533mm/min (21ipm) feedrate in contrast to 457mm/min (18ipm) used in the other five cases shown.

Figure 8 shows data collected while cutting at high preheat and cutting oxygen, but at lower feedrates. These produced less severe bottom-edge dross, but substantial intermittent top-edge dross. To aid interpretation of these data, they are shown in color

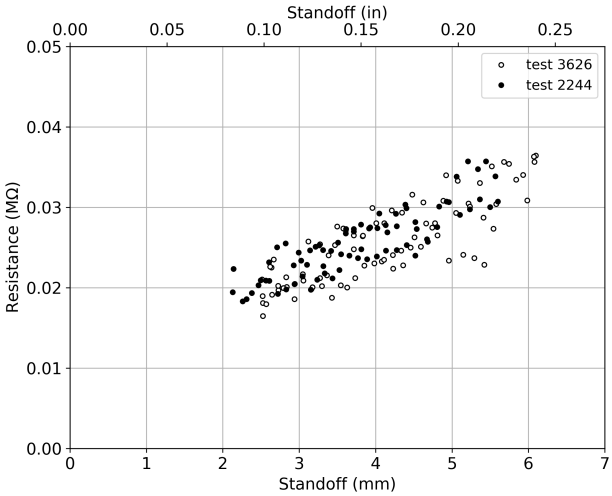

FIGURE 6. Resistance versus standoff; 1/2-inch steel, 660mm/min and 610mm/min, high preheat, high cutting oxygen

with the darkest portion of the curve representing data immediately after pierce and the lightest portion of the line representing data at the end of cut. Unlike the last data sets, these represent a definite hysteresis loop. The one loop that diverges somewhat from the others was conducted at higher feedrate.

Finally, Figures 9 and 10 show similar hysteresis loops while cutting 1/4-inch plate. These cuts were conducted under the same conditions as Figure 4 (low preheat, nominal cutting pressure). Figure 9 shows cuts with 406mm/min (16ipm) feedrate and Figure 10 shows cuts with 533mm/min (21ipm) feedrate. Both of these datasets demonstrate a severe repeatable hysteresis loop with high resistance early in the cut and low resistance late in

Copyright © 2021 by ASME

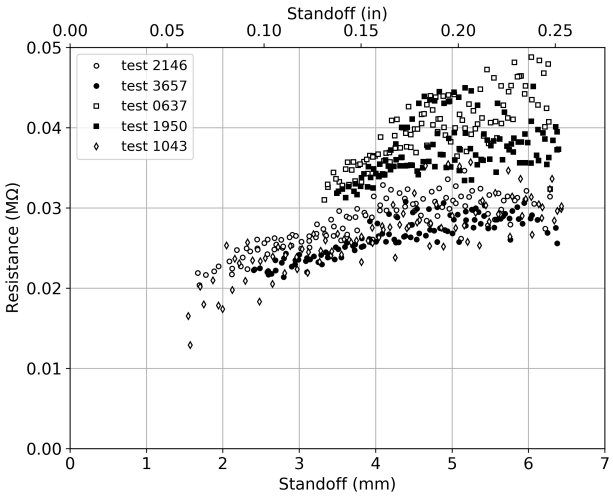

FIGURE 7. Resistance versus standoff; 1/2-inch steel, 457mm/min and 533mm/min, high preheat, high cutting oxygen, .77 and .80 f/o mixtures.

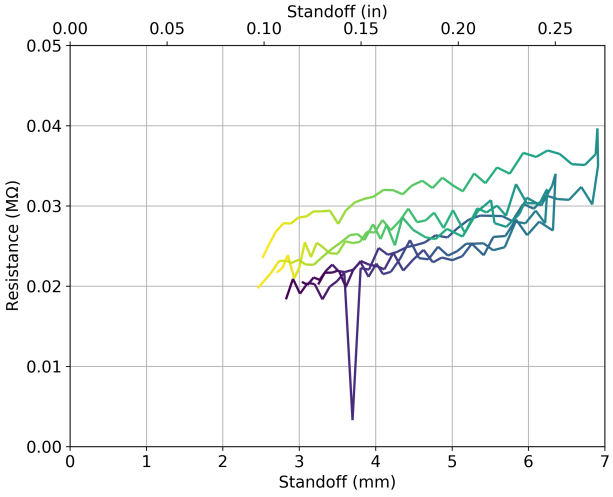

FIGURE 8. Resistance versus standoff; 1/2-inch steel, 457mm/min and 508mm/min, high preheat, high cutting oxygen. Three tests are shown starting proceeding from dark to light color. Tests 42641, 4833, and 5105 shown.

the cut.

These plots alone represent twenty data sets exploring five independent variables. To help organize the scope of the study, their results are summarized in Table 1. Results are characterized using letter codes to identify plots with hysteresis (H), scatter (S), or linear (L) behaviors. The cut quality is characterized as good (G), top-edge dross (T), intermittent top-edge dross (IT), or cold kerf (C) causing tearing or bottom-edge dross.

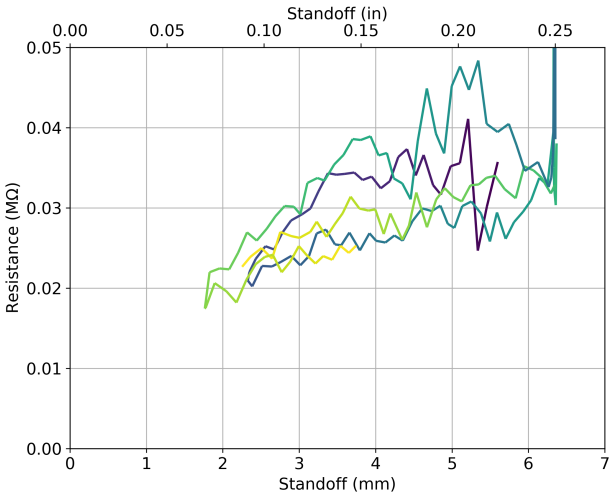

FIGURE 9. Resistance versus standoff; 1/4-inch steel, 406mm/min, low preheat, nominal cutting oxygen. Cut proceeds from dark to light color. Tests 1006 and 4931 shown.

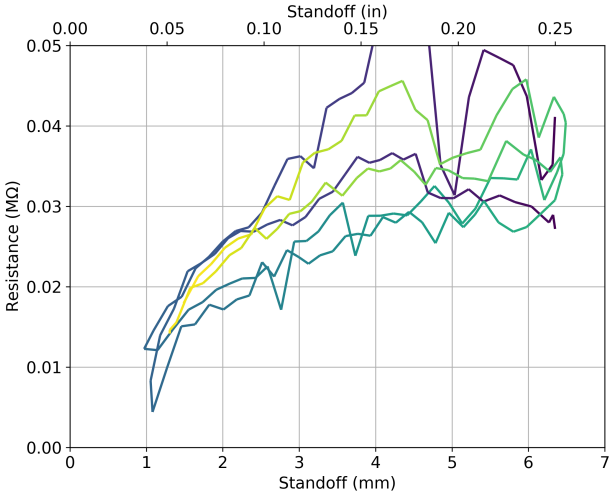

FIGURE 10. Resistance versus standoff; 1/4-inch steel, 533mm/min, low preheat, nominal cutting oxygen. Cut proceeds from dark to light color. Tests 2531 and 3817 shown.

3.2 Loss-of-cut

In seven data sets, loss-of-cut (LOC) events occurred. When a cut is lost, the oxidation of iron in the kerf of the cut halts, the kerf cools, and the torch proceeds over solid non-burning plate. In all seven data sets, there was an abrupt rise in the flame resistance coinciding with LOC.

Figure 11 shows the harmonic components of the voltage signal throughout one of those tests. The fundamental (black) is proportional to the resistance signal and relatively large harmonics (blue and red) indicate that the measurement is nonlinear and

Copyright © 2021 by ASME

TABLE 1. A summary of figures representing successful cut data. Behaviors (Beh.) are encoded as L: linear, LS: linear with scatter, H: hysteresis, and HS: hysteresis with scatter. Cut quality (Qual.) is encoded as G: good, D: top-edge dross, ID: intermittent top-edge dross, C: cold kerf.

Fig.	Beh.	Qual.	Thick	Feedrate	Preh.	Cut P.	Mix
			mm	mm/min	N/H	L/H	F/O
4	L	G	13	406	Nom	Low	.77
5	LS	D	13	305	High	Low	.77
6	LS	D	13	610,660	High	High	.77
7	LS	D	13	457,533	High	High	.80,.77
8	HS	ID	13	457,508	High	High	.77
9	H	ID	6	406	Nom	Low	.77
10	HS	C	6	533	Nom	Low	.77

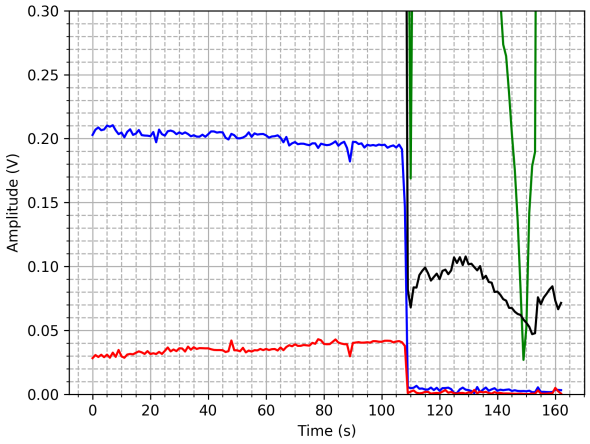

FIGURE 11. Harmonic components durring a loss-of-cut event. Green: DC (0Hz), Black: Fundamental (10Hz), Blue: First Harmonic (20Hz), Red: Second Harmonic (30Hz).

therefore invalid. In this test, ignition occurred around 110 seconds, after which the measurement quickly became quasi-linear. As standoff declined, the fundamental voltage (proportional to resistance) declined linearly. At about 157 seconds, there was an abrupt rise in voltage with no corresponding rise in harmonics, indicating that the measurement was still quasi-linear.

This behavior is consistent with every LOC event observed during this study; a rise in resistance with no corresponding rise in harmonics. This is especially surprising since one such event occurred due to blockage of the preheat channels at extreme low standoff (less than 1mm or .04in). These data indicate that the rise in flame resistance prior to LOC is genuine and not an artifact

FIGURE 12. Photograph of the tip after test 2603. Dross adhered to the torch tip.

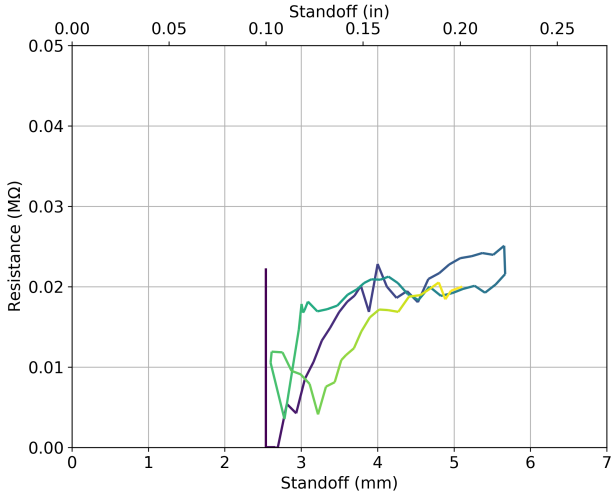

FIGURE 13. Flame resistance versus standoff probe for test 2603, durring which dross adhered to the tip immediately after pierce.

of a reduction in saturation currents.

3.3 Torch tip damage

In one test, a pierce operation at low standoff emersed the torch tip in a pool of molten metal for a moment, and dross adhered directly to the tip, as shown in Figure 12. In Figure 13, the resistance can be seen dropping precipitously immediately after the cut began. As soon as the torch progressed out of the dross pool, the resistance resumed an astonishingly self-consistent characteristic.

Copyright © 2021 by ASME

4 Discussion

Across all of the data presented in these results, as cut quality degraded, so did the correlaiton between flame resistance and torch standoff. This section explores the mechanisms for that degredation. As this section establishes, preheat flow rate and cutting oxygen pressure do not impact the flame resistance directly, but their effects are seen indirectly through their impact on the plate. Only fuel/oxygen ratio has an important direct impact of flame resistance, seen clearly in Figure 7.

4.1 Mechanisms for reduction in resistance

In Figures 4 and 5 there was a reduction in resistance at high standoff, causing the resistance-standoff curve to flatten. Studies to date suggest three mechanisms for such a reduction in flame resistance: (1) a decrease in flame resistivity due to an increase in chemical action at the work, (2) reduction of the length of the electrical path, or (3) leaning of the flame mixture.

The latter may be rejected immediately since drift in flow rates of this kind would never be so highly repeatable. Reduction in flame resistivity due to an increase in charge carrier density has been shown to be a phenomenon while preheating steel samples [5], but what would be the mechanism for such a thing while increasing standoff in a cut? The plate and kerf should be (if anything) growing colder, so the reaction rate in the kerf should be declining. This leaves only the reduction of electrical path length due to the formation of top edge dross.

Figure 14 shows frames from near infrared video shot of test numbers 1605 and 5240, as shown in Figure 4. At low standoff, molten metal is constrained to the walls of the kerf, but at at higher standoff, rows of liquid metal can be seen rising out of the kerf on either side. The onset of top-edge dross around 4mm (0.15in) standoff can be found consistently across these three data sets. The deviations in resistance are consistent with dross globules 1 or 2mm (.05 or .1in) tall. Finally, the increase in noise under these conditions is consistent with the cyclic clearing and reformation of the dross globules.

Figure 15 shows frames from test 3626 (Figure 6) that typify the cyclic formation and clearing of large dross globules. Though heavily unsteady, this phenomenon occurs continuously and repeatably under these conditions, resulting in a highly unsteady reduced electrical path length.

A similar examination of the hysteresis loops in Figure 8 shows that large quantities of dross consistently formed on the portion of the cuts where standoff was rising but not when falling. These conditions seem to have accidentally created a situation where the slight angle between the torch and the plate impacted the transport of dross ahead of the kerf differently depending on the direction of travel. The divergence of one of the three curves appears to be the only portion of one cut that experienced little top-edge dross, allowing it to resume the resistances observed in Figure 4.

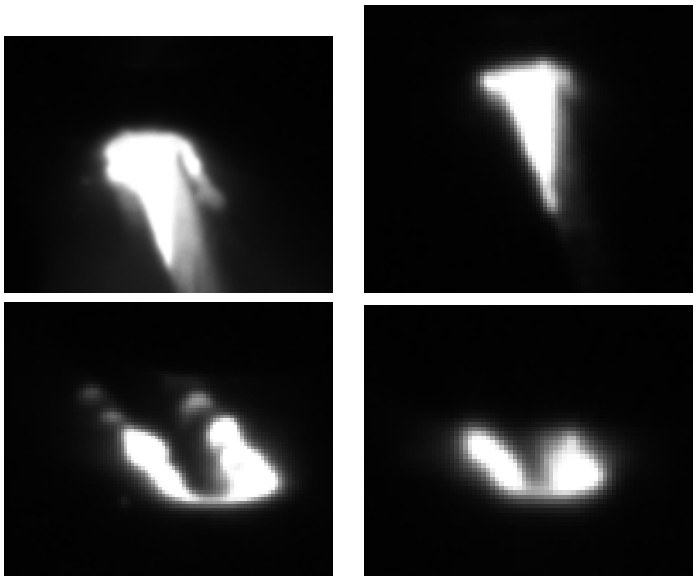

FIGURE 14. Near-infrared images during high- and low-standoff conditions in test 1605 (top) and 5240 (bottom) while cutting at high- (left) and low-standoff (right). Tests are from Figure 4.

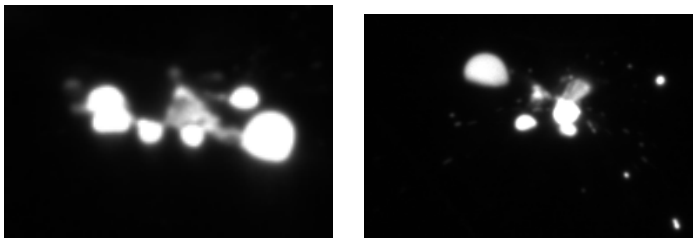

FIGURE 15. Near-infrared images during test 3626. Tests are from Figure 6.

4.2 Mechanisms for increases in resistance

Studies to date suggest four possible mechanisms for an abrupt rise in resistance while cutting: (1) a drop in positive saturation current artifically increases the resistance signal by forcing the current to be driven against a saturation, (2) an increase in the flame resistivity due to a reduction in charge carriers generated by chemical action at the work, (3) a layer of non-conducting cool oxygen forms between the flame and the work, restricting the flow of ions, and (4) changes in flow rate richens the preheat flame mixture.

Since none of the increases in resistance were accompanied by corresponding increases in superharmonics, drops in saturation current can be rejected. This is somewhat surprising since saturation currents are known to decrease when the chemical reaction at the work declines. Since changes in flow rates were not responsible for the loss of cut conditions, such a coincidental drift in flow rate in all seven tests is also an unacceptable hy-

Copyright © 2021 by ASME

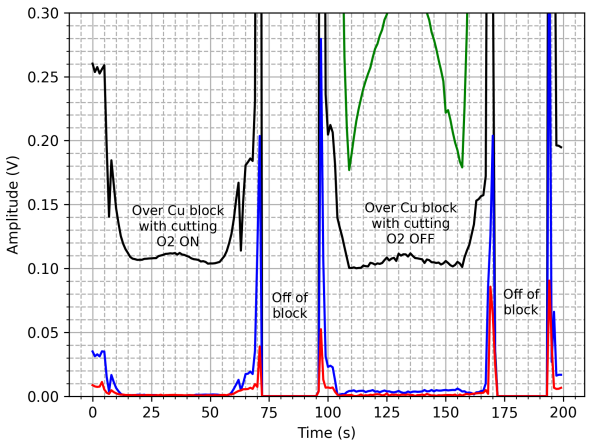

FIGURE 16. Test showing resistance as a function of time as the torch was moved over a copper block first with and then without cutting oxygen

pothesis. Instead, one is left with only two tennable explanations consistent with the data presented so far.

If a cool layer of oxygen is responsible for the increase in resistance, then there should be a subtantial increase in resistance when cutting oxygen is applied over any nonreacting surface. To test the hypothesis, a water-cooled copper block was placed with its edge precisely beneath the center of the torch so that half of the preheat flamelets did not interact with it. The cutting oxygen was applied and the torch was slowly (50mm/min or 2ipm) moved 25.4mm (1in) to the center of the copper block and back. There, it was allowed to dwell for four seconds before moving 13mm (.5in) off of the block and back so that none of the torch's gases were interacting with the block for a portion of the test. The cutting oxygen was halted, the torch was allowed to dwell for another four seconds, and then the entire process was repeated without cutting oxygen.

In this way, the process of the torch progressing out of the kerf of a lost cut and over a nonreacting body with cutting oxygen activated may be loosely simulated. The impact of the cutting oxygen is assessed by comparing the result against similar measurements without the cutting oxygen.

The data collected in Figure 16 were collected with 3.8mm (.15in) standoff, nominal cutting oxygen pressure (3.1bar or 45psig), and high preheat (16.8L/min or 35scfh). The test was repeated three times with comparable results. Data without the cutting oxygen show a higher first harmonic, suggesting that the positive saturation current has dropped low enough to impact the resistance measurement somewhat. There is a slight increase in resistance as the torch moved over the copper block because the block was not entirely level with the torch motion.

These data withstanding, it is impossible to accept that the cutting oxygen forms an insulating layer. There is no significant difference between cutting oxygen off and cutting oxygen on conditions; even when the torch is positioned over the block edge.

The remaining conclusion is that these increases in resistance are due to a change in the plasma resistivity. The factors that impact a plasma's resistivity are widely known, and have been studied in the oxyfuel flame [1,2,11]. If the flame electrical properties are imagined to be uniform, the total flame resistance may be estimated as

$$R = \frac{L}{A q_e n_e \mu_e}. \tag{1}$$

Here, n_e, μ_e, and q_e are the number density, electrical mobility, and charge of free electrons. The physical dimensions of the flame are represented by length, L, and cross-sectional area, A. This uniform approximation gives excellent order-of-magnitude agreement with direct measurements [1,2,9], but a non-uniform formulation has also been presented in [11]. These lead to the same important result: the flame resisistivity is primarily influenced by variations in the number density of free electrons.

4.3 Links to poor cut quality

There are two broad classes of conditions that caused poor cut quality in these tests: (1) excessive feedrate or insufficient heating cause the cutting mode to transition from primarily burning to a cyclic clearing of molten steel from the kerf, and (2) insufficient feedrate or excessive heat causes top-edege rounding and top-edge dross.

As discussed above, Figures 8, 9, and 10 all represent data collected with severe top edge dross on passes with rising standoff, causing a hysteresis loop. The formation of molten metal globules durring cut reduced the path length between the torch and the work, reducing the resistance. This effect is most clear at high standoff in Figure 4 and on rising passes in Figure 8, but it is clearly complicated with a second effect in Figures 9 and 10.

Ideally, oxyfuel cutting should primarily be the process of burning away steel in the oxygen jet, but at excessive speeds, the reaction rate slows and the mechanism of cutting transitions to a "blowing" away of molten unburned metal in the kerf. Under these conditions, the cut is very nearly lost, and cutting under this condition is occasionally referred to as "tearing" (inspired by jagged appearance of the cut face). Much of the unburned molten steel is allowed to reweld underneath the plate, causing a tenacious "high-speed" dross.

This mode of cutting comes along with a dramatic reduction in the rate of oxidation in the kerf, which is especially visible when the high resistances observed when Figures 9 and 10 are compared with Figure 4. Chemical action in the kerf is a major source of free electrons, causing the flame resistivity to drop by

Copyright © 2021 by ASME

as much as a factor of three from non-cutting conditions [2]. If the reaction rate in the kerf is reduced, it seems obvious that there would be a corresponding impact on the flame's resistivity.

This is confirmed in Figure 9, which was deliberately produced under the same conditions as Figure 4, but heat transfer ahead of the cut is slower in thin plate than in thick plate. Furthermore, thin plates' kerf is shallower, so the heat released by oxidation of steel is less, making the process more dependent on heat from the preheat flame and more sensitive to convection and radiative losses at the surfaces. At high standoff, the plate was at its coldest, so the reaction rate in the kerf was suppressed, causing elevated resistance. The effect is severely magnified by increasing the feedrate in Figure 10, but the signal was able to recover somewhat during the cut as the plate warmed.

5 Conclusions

When the electrical resistance of the oxyfuel flame is defined as the quasi-linear slope relating voltage to current in the regime between positive and negative saturation, it may be said to be impacted by two factors: (1) the resistivity of the plasma, and (2) the electrical path length between the torch and work piece.

During loss-of-cut events, or when cutting at high feed rates in a "tearing" mode, the electrical resistivity rises. This is due to a reduction in the oxidation reaction rate in the kerf, causing a deficiency of free electrons in the flame.

Fuel/oxygen ratio was the only independent parameter in this study that had a direct impact on flame resistance. Otherwise, changes in feed rate, flow rates, or pressures only impacted the flame resistance indirectly through their impacts on the cutting process. The formation of top-edge dross reduced the electrical path length and slowing the reaction rate in the kerf suppressed the formation of charge carriers.

Under proper quality cutting conditions, the use of flame resistance as a measure of of standoff is reliable and repeatable. When the quality of the cut is compromised, the reliability of the standoff measurement is reduced. Under ideal conditions, when the flame resistivity is stable (Figure 4), the uncertainty of a standoff measurement deduced from flame resistance is about $\pm$ 0.3mm (.015in).

When the flame resistivity fluctuates heavily or the formation of top-edge dross corrupts the measurement, uncertainty degrades to $\pm$ 1mm (.040in) or worse. While the authors regard this as disappointingly high uncertainty, it is astonishingly consistent with current commercial offerings.

Clearly, there are complications of which CNC system developers need to be aware when implementing the measurement, but these results appear quite optimistic for implementation. Maintaining tight control on torch height is important for maintaining high quality cuts, but when the cut quality is already compromised standoff distance becomes far less critical. In such a situation, the standoff measurement is only needed to prevent a torch crash event, for which even the highest uncertainties observed are quite adequate.

There appear to be four advantages to flame resistance sensing over capacitive sensing:

1. It appears that in good cutting conditions, the flame resistance measurement offers superior height measurement uncertainty.
2. Unlike capacitive height measurements, uncertainty in the flame resistance standoff measurements degrades when the cut quality is already quite poor do to other process problems.
3. Capacitive measurements are not capable of operating so near to the plate edge, as was done in all of these experiments.
4. Damage to the torch tip that threatens to compromise the measurement is likely to compromise the process anyway.

Acknowledgements

The work presented here was made possible by award 1900698 from the National Science Foundation.

This work was also supported in part by a donation of steel by Curry Rail Services Inc. located in Hollidaysburg, PA.

REFERENCES

[1] Martin, C., Leonard, C., and VonFricken, J., 2017. "A study of the electrical characteristics of an oxy-fuel flame". *Experimental Thermal and Fluid Science,* ***88***, pp. 65–72.

[2] Pond, T. L., and Martin, C. R., 2020. "Electrical characteristics of the oxyfuel flame while cutting steel". *Experimental Thermal and Fluid Science,* ***112***, p. 109985.

[3] Messer sensomat-pan. https://us.messer-cutting.com/.../Sensomat_Pan_01.pdf. accessed: Jan 26, 2021.

[4] Mott, C., Chouinard, A., and Harding, R., 1944. Torch device. US Patent 2364645, Dec. National Cylinder Gas Co. 266/23.

[5] Martin, C. R., 2018. "A study of ion currents in an oxyfuel flame due to work surface chemical action". *Experimental Thermal and Fluid Science,* ***98***, pp. 239–250.

[6] Martin, C., 2017. "Replacing mechanized oxyfuel cutting sensors with ion current sensing". In Proceedings of the ASME 2017 Manufacturing Science and Engineering Conference, pp. MSEC2017–2789.

[7] Martin, C., 2018. "Electrical signatures for chemical action at the work surface in an oxyfuel flame". In Proceedings of the ASME 2018 Manufacturing Science and Engineering Conference, pp. MSEC2018–6354.

[8] Martin, C. R., Pond, T., Tomas, J., Schmit, J., Miguel, E., Untaroiu, A., and Xu, K., 2020. "Semiconductor aspects

Copyright © 2021 by ASME

of the oxyfuel cutting torch preheat flame, part i: Measurements between torch and work". In Proceedings of the Manufacturing Science and Engineering Conference. [In-Press].

[9] Martin, C. R., Untaroiu, A., and Xu, K., 2020. "Spatially resolved ion density measurements in an oxyfuel cutting flame". *Combustion Science and Technology,* ***0***(0), pp. 1–16. [IN PRESS].

[10] Xu, K., Untaroiu, A., and Martin, C., 2020. "Simulation of ion current in oxyfuel flame subject to an electric field". In Proceedings of the ASME International Mechanical Engineering Congress and Exposition, p. 24601.

[11] Martin, C. R., Untaroiu, A., and Xu, K., 2020. "A one dimensional model for ion transport in a flame with two absorbing surfaces". *Combustion Theory and Modelling,* ***25***(1), pp. 22–43.

Copyright © 2021 by ASME